

# Personalized Airway Trees from a Generative Model, Lung Atlas, and Hyperpolarized Helium MRI.

William Mullally<sup>1</sup>, Aladin Milutinovic<sup>2</sup>, Margrit Betke<sup>1</sup>, Mitchell Albert<sup>3</sup>, Kenneth Lutchen<sup>2</sup>

<sup>1</sup> Department of Computer Science, Boston University, USA

<sup>2</sup>Department of Biomedical Engineering, Boston University, USA

<sup>3</sup>Hyperpolarized Noble Gas MRI Laboratory, Brigham and Women’s Hospital, USA

**Abstract**—Biomedical researchers are actively interested in building anatomically explicit computational models of the lung to further their understanding of pathologies, for example asthma, which affect the human body. Current methods have relied on a generic lung airway model which may not accurately reflect the physiology of a given subject. Patient specific models are needed to overcome this limitation. We propose a method for creating personalized models of the lung from Hyperpolarized Helium MRI images (Hyp. <sup>3</sup>He MRI). As Hyp. <sup>3</sup>He MRI images are of insufficient resolution to identify lung lobes, an estimate of lung lobe locations is obtained by registering a lung atlas to the MRI images. We then use a generative technique to create a lung airway model within the estimated lung lobe volumes. Initial testing indicates significant differences in predictions of lung function between the personalized model our approach generates and a generic airway model.

## I. INTRODUCTION

The human lungs are a complex system of bifurcating airways that have been studied using a variety of models [3], [5], [6], [7]. In particular, we are interested in computational models that can shed light on how diseases affecting lung airways result in loss of lung function. Previous computational work by Tgavalekos et al. [7] invoked an approach coined Image-Function Modeling (IFM) to investigate which airways in asthma cause degradation in lung function. Tgavalekos et al. used PET ventilation images and a generic three-dimensional lung model developed by Tawhai et al. [6] to predict which airways in the model contribute to the degradation of lung function. The lung model represents individual airways as a hierarchy of bifurcating cylindrical tubes – the trachea bifurcates into two airways, which then bifurcate systematically to fill the volume of the lung space. The diameters of the airways are randomized based on observed mean and standard deviation of airway diameters found for that particular generation. Tgavalekos et al. examined lung function by mapping ventilation defects in the corresponding areas of the three-dimensional lung model. This mapping was achieved by scaling the Tawhai model to fit into the subject’s lung cavity. They then determined which airways had to be closed to cause such dropouts in ventilation while matching oscillatory mechanics of the lungs.

Resistance and elasticity of the lungs are important measures of lung function and can be routinely measured in humans as well as in computational models [4]. In our work,

the lung airways are modeled as cylindrical elements. The resistance and inertance are due to tubular airflow. The smaller the airway, the higher is the resistance. The inertance results from the momentum of air. The compliance is due to the elasticity of wall and parenchymal tissues. Both resistance and elastance can be numerically approximated from Tawhai’s model. Due to the varying impedance of each path down the airway tree, various frequencies of oscillation will produce varying resistance and elastance. Tests on the model amount to predictions of a subject’s lung function. These predictions can be compared to measurements from that subject and result in a deeper understanding of the mechanics of the lungs.

To date, the IFM approach has been implemented with only the generic lung model of Tawhai et al. [6]. This single model may not accurately represent lung function in all subjects. Therefore it is desirable to construct a personalized 3D lung model for a each subject to predict which airways close and how the remaining airways constrict in that subject. Zidowitz et al. [9] have proposed a method for personalizing the Tawhai model. Their approach relies on features seen in high resolution CT scans that are not apparent in other imaging modalities. Also, Zidowitz’s approach must be given lung lobe locations. We propose a method for generating such patient specific three-dimensional lung airway models by automatically determining the lung lobe locations.

The three-dimensional lung model of Tawhai et al. was built using a generative approach within a specific lung volume. For an anatomical accurate result, this model should be generated to fit into the volumes of the lung lobes rather than the lungs as a whole. Unfortunately, images in which ventilation defects are easily detected, for example, PET and the Hyp. <sup>3</sup>He MRI images (Fig. 1) used in this paper, are not of sufficient resolution to allow for the easy localization of lung lobes. Estimates on the lung lobe locations are therefore obtained by mapping the lung fissure boundaries from a lung atlas into the lung volumes obtained from the MRI images. We then use Tawhai’s approach to generate a personalized model to fit into these volumes. We detail our method below and show a comparison of the Tawhai model to our patient specific model.

## II. METHOD

The initial input to our algorithm is a Hyp. <sup>3</sup>He MRI of the lung. The MRI consisted of coronal images with  $1.2 \times 1.2 \times 13$  mm resolution. Our goal is to construct an anatomically

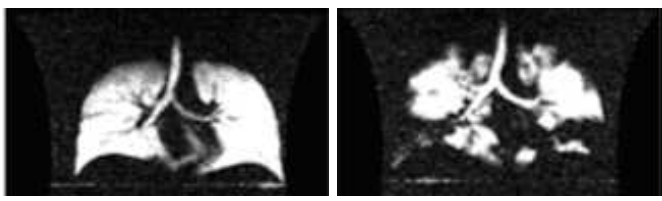


Fig. 1. Hyp.  $^3\text{He}$  MRI of the lung a healthy individual (left) and a constricted asthmatic (right). Brightness relates to degree of ventilation. In the healthy lung, all regions of the lung are ventilating normally. In the asthmatic lung, large regions of the lung are receiving little or no ventilation.



Fig. 2. Cryosection image from the Visible Human Data Set. Lung fissures are circled in white. Lung lobes and lung boundaries were hand marked to build a lung atlas.

feasible model of the lung lobes within the boundaries of the imaged lung. Our algorithm proceeds in the following steps. 1) Segment the lung volumes from the MRI scan. 2) Register a lung atlas to these lung volumes. 3) Divide the lung volumes into lobes based on the lobes from the lung atlas. 4) Generate a personalized airway model into the lung lobe volumes.

In Hyp.  $^3\text{He}$  MRI of healthy lungs and non-constricted asthmatics, features like the trachea, carina, and lung boundaries stand out sharply against the image background. To segment out the lung volumes, we first apply a threshold to the MRI scan to isolate areas of high ventilation. Morphological operators are then applied to fill small holes in the resulting volumes. The trachea and bronchi are removed by hand. What remains is a binary mask of the lung volumes. We also automatically generate a cloud of points at the boundary of this volume to represent the surface of the lung.

We map a lung atlas with marked lung lobes to these lung volumes. The atlas we use was generated by hand marking cryosection images from the Visible Human Project [8]. The visible human project shows axial images of a human (see Fig. 2) with resolution  $1.32 \times 1.32$  mm. We use images at 10 mm intervals in the cranial-caudal direction to build our atlas. Both the lung boundary and the fissures separating the lung lobes are marked, and the volumetric masks of the lung lobes and a cloud of points on the lung surface are created.

We then align the lung atlas with the MRI scan by using an iterative closest point (ICP) algorithm [1] on the lung surfaces [2]. ICP is sensitive to the initial orientation of the surfaces to be registered, so we first perform a course manual alignment of the two volumes. Since the MRI images are coronal and the visible human project has axial images, this manual alignment amounts to a 90 degree rotation of the atlas so that the two

datasets have the same general cranial-caudal direction. We then use the ICP algorithm to compute an affine transformation of the lung surface into the atlas surface.

Once this alignment is complete, we can apply the same transformation that aligns the lung surfaces to map each voxel in the MRI lung volume to a corresponding voxel in the visible human dataset. Our goal in this step is to approximate the lung lobes in the MRI scan from the atlas. We take two passes of the lung volume to assign all voxels to a lobe. In the first pass, we label each voxel in the MRI volume as belonging to the same lobe as its corresponding voxel in the lung atlas. An affine transformation is not sufficient to align all voxels of the lung with voxels in the atlas. Because of differences in overall size and shape of the lungs and the atlas, some voxels in the MRI volume may map to voxels that are outside of the atlas. Therefore, we pass through the lung volume a second time to assign these unlabeled voxels to a lobe. For each unlabeled voxel we find its nearest voxel that was labeled in the first pass of the lung volume and give it the same label. Grouping all voxels by their label then results in separate volumes for each lung lobe (Figure 3).

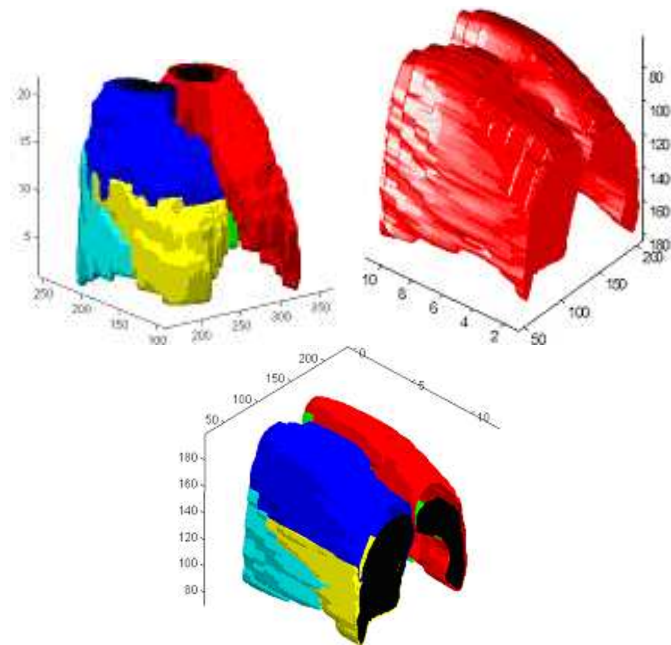


Fig. 3. Top Left: A surface model of the lung lobes from the visible human data set. Top Right: A surface model of the lungs from a MRI image. Bottom: A model of lung lobes in the MRI volume achieved by mapping the visible human data set into the MRI volume.

We then generate the airway tree model into the resulting lung lobe volumes following the approach of Tawhai et al. [6]. The algorithm starts from the initial position of the trachea and creates branches that move in the direction of the lung and then in the direction of each of the lung lobes. Volumes are then cut in two, and smaller branches are created that move to the centroids of these smaller volumes. This process repeats itself until branches become either too short or the volume they would move into becomes too small.

In addition to the lung lobes there are several significant parameters to this algorithm for which we did not use the

same values in the Tawhai model. This includes the number of points in a volume required for terminating a branch, the minimum length of a branch before it becomes a terminal branch, the length and diameters of airways at each generation of the tree, and the starting location of the trachea. The position of the starting point of the trachea is approximated by placing it 30 mm above the lung volume and 20 mm towards the front of the lung. The end point is located at the center of the volume of the lung, and is elevated 20 mm toward the apex. The diameter of the trachea is also different, 16 mm for Tawhai and 20 mm for our generated model. The diameters of airways used in this work are values from Tgavalekos et al. [7] where total lung volume is assumed to be 3 liters at functional respiratory capacity. Values for determining the termination of a branch were obtained using a sensitivity study.

### III. RESULTS

We tested our algorithm on a single Hyp.  $^3\text{He}$  MRI scan of healthy lungs. Figure 4 visually shows the difference between the generic airway tree provided by Tawhai et al. and the results of our algorithm.

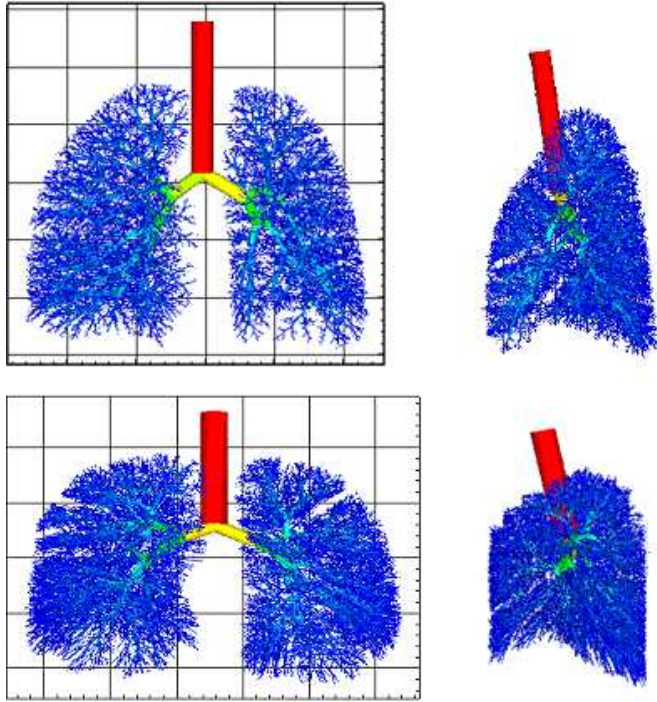


Fig. 4. The generic airway tree of Tawhai (top) vs. personalized airway tree (bottom). Both a frontal and sagittal view are shown. The overall shape of the two models is significantly different and the personalized model is less symmetric.

The sensitivity of two algorithm parameters was tested: the number of points in a subvolume required for terminating a branch and the minimum length of a branch before it becomes a terminal branch. These parameters control when a branch is determined to be a terminal branch. The number of points required in a subvolume for a terminal branch was varied from 3 to 6 in integer increments, keeping the minimum length of a branch 1.2 mm. Figure 5 shows the results of varying the number of points. Notice that with increasing number

of points, there are fewer airways generated. The number of generations also decreases. Figure 5 indicates that there is a similar number of branches up until generation 13 or 14 for all values of the number of points. After generation 14, airways terminate faster for a higher value of the number of points.

Another parameter tested was the minimum length of the branch. The minimum length of the branch was varied from 1.1 mm to 1.4 mm in 0.1 mm increments, while keeping the number of points required for terminating the branch equal to 5 (Figure 5). The larger the minimum length of the airway, the fewer numbers of airways are generated. Changes to the minimum length of the airway, however, do not cause as large changes in the number of airways as varying the minimum number of points. Together, these two parameters can be varied to fine-tune the number of airways that are generated.

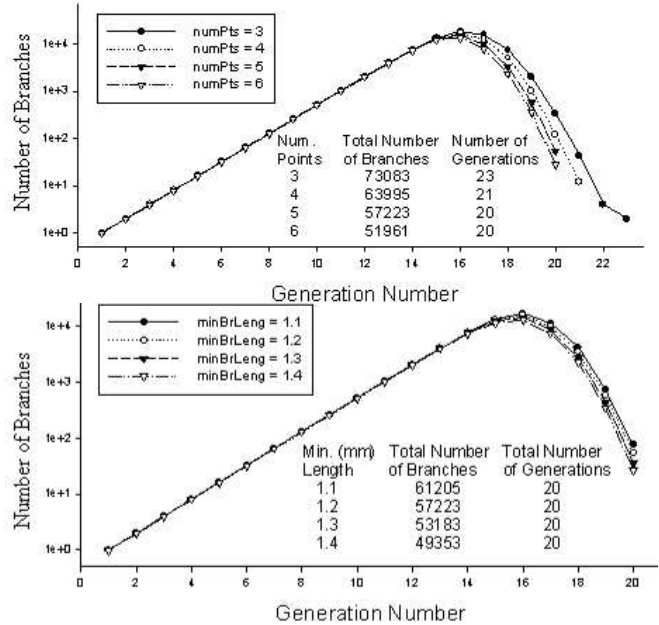


Fig. 5. Top: The distribution of branches for various numbers of points required for terminating the airways; constant minimum branch length is 1.2 mm. Bottom: The distribution of branches for various lengths of airways required for terminating the airways; constant minimum number of points is 5.

We also performed a series of computational oscillatory mechanics tests [7] to compare our model and the generic Tawhai model. To test how the patient-specific airway tree compared to the generic tree, a series of constriction patterns were imposed on both trees. The trees were constricted by 0, 20, 40, and 60 percent with varying standard deviation of 0, 20, 40, and 60 percent. A total of 16 simulations resulted for each model. From these simulations variability in resistance and elastance between the two models was observed. The baseline condition is when no airways are constricted ( $M=0$ ,  $SD=0$ ). Heterogeneous constriction consists of a low mean of constriction with a high standard deviation ( $M=20$ ,  $SD=60$ ), and homogeneous constriction consists of a high mean of constriction with a low standard deviation ( $M=60$ ,  $SD=0$ ). Constriction patterns are achieved by progressing through each airway that is below generation 12 in the model and reduces

the diameter by a percentage drawn randomly from a Gaussian distribution of the given mean and standard deviation.

Selected results are shown in Figure 6 for the personalized model (solid lines) and the Tawhai model (dashed lines). Panels A and B in Figure 6 show the impact of increasing standard deviation with mean constriction equal to zero. In general, with increasing standard deviation, the resistance becomes more frequency dependent and elastance increases at low frequencies. With a high enough standard deviation, the elastance jumps up indicating that some airways have been closed. There is some frequency dependence for elastance as well; however, not as much as with the resistance. The elastance of the Tawhai model tends to be very similar at low frequencies, but decreases more rapidly with frequency for every standard deviation. Panels C and D in Figure 6 show the effect of increasing mean constriction with standard deviation equal to zero (homogeneous constriction). A large difference between the two models occurs where the personalized model has increased elastance. This increased elastance suggests that there is more shunting occurring in the personalized model.

Finally, panels E and F in Figure 6 show both the mean and standard deviation changing at the same time. The elastance of the personalized model tends to be very similar to the Tawhai model at low frequencies, but increases more rapidly with frequency for every standard deviation. The two models are similar in frequency dependence of the resistance. However, they slightly differ in the magnitude of the resistance.

Our results indicate that the modeling methods in this work generate airway trees that are notably different from the original Tawhai model. When comparing mechanics simulations with the general Tawhai model, the simulations revealed an increased resistance and less frequency dependence at heterogeneous constriction. Also, the model generated in our test is less symmetric than the original Tawhai model, which is due to the differences in lung cavities of individual subjects. These differences indicate that it may be important to have personalized models.

#### IV. CONCLUSION

Using IFM, Tgavalekos et al. have shown that constriction of small airways (less than 2 mm in diameter) cause lung function impairment that is present in asthmatics. The 3D model used by Tgavalekos et al. has been a generic Tawhai airway model. Our method has made it possible to generate airway models that are patient specific. The patient-specific model is different from the original Tawhai model in size and shape. The personalized model provides a better characterization of airways of the particular individual since it is generated into the space from which ventilation is mapped. Our tests show that there are meaningful differences between the personalized model and the original Tawhai model in the number of airways, their distribution across generations, and the simulated mechanics. Using personalized instead of generic airway models may significantly improve researchers' ability to understand lung mechanics.

Future studies should more closely investigate how changes in the airway distributions and diameters affect the IFM simulations. Other sensitivities with regard to the number of

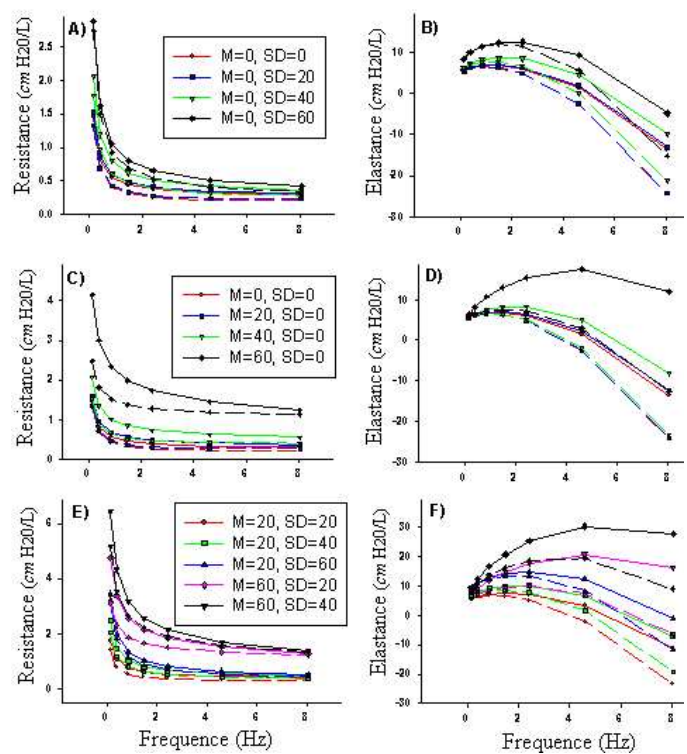


Fig. 6. Mechanics simulation of the resistance and elastance of the lung over a range of oscillatory frequencies for patterns of various mean and standard deviation of constriction of the airways below the 12th generation. Dashed lines represent the Tawhai model and solid lines represent our personalized model.

terminal airways should also be investigated. Future work may also improve the mapping of the lung lobes from the atlas to the MRI scan, perhaps by using a non-rigid approach or by using a statistical atlas.

#### REFERENCES

- [1] P. J. Besl and N. D. McKay. A method for registration of 3-D shapes. *IEEE Trans Pattern Anal Mach Intell*, 14(2):239–256, 1992.
- [2] M. Betke, H. Hong, D. Thomas, C. Prince, and J. P. Ko. Landmark detection in the chest and registration of lung surfaces with an application to nodule registration. *Med Imag Anal*, 7(3):265–281, Sept. 2003.
- [3] J. Garrity, W. Segars, S. Knisley, and B. Tsui. Development of a dynamic model for the lung lobes and airway tree in the NCAT phantom. *IEEE Trans Nucl Sci*, 40(3):378–383, 2003.
- [4] K. Lutchen, A. Jensen, H. Atileh, D. Kaczka, E. Israel, B. Suki, and E. Ingenito. Airway constriction pattern is a central component of asthma severity: the role of deep inspirations. *Am J Respir Crit Care Med*, 164(2):207–215, 2001.
- [5] N. Nowak, P. Kakade, and A. Annapragada. Computational fluid dynamics simulation of airflow and aerosol deposition in human lungs. *Ann Biomed Eng*, 31:374–390, 2003.
- [6] M. Tawhai, A. Pullan, and P. J. Hunter. Generation of an anatomically based three-dimensional model of the conducting airways. *Ann Biomed Eng*, 28(7):793–802, 2000.
- [7] N. T. Tgavalekos, M. Tawhai, R. S. Harris, G. Musch, M. Vidal-Melo, J. G. Venegas, and K. R. Lutchen. Identifying airways responsible for heterogeneous ventilation and mechanical dysfunction in asthma: An image-function modeling approach. *J App Physiol*, 31(4):363–373, 2005.
- [8] US National Library of Medicine, Visible Human Data Set. [http://www.nlm.nih.gov/research/visible/visible\\_human.html](http://www.nlm.nih.gov/research/visible/visible_human.html). Retrieved in 2005.
- [9] S. Zidowitz, A. H. Schmidt, A. Kriete, S. Krass, and H.-O. Peitgen. Steps toward a patient individual geometric model of the bronchial-tree used for functional simulations. In *Proc. SPIE Medical Imaging 2004: Physiology, Function, and Structure from Medical Images*, pages 125–131, 2004.